IDENTIFYING FAILURE INITIATION IN AUTOMOTIVE STRUCTURES MADE OF NCF REINFORCED COMPOSITES FOR HOT SPOT ANALYSIS

Henrik Molker[1], Renaud Gutkin[2], Silvestre Pinho[3] and Leif E. Asp[4]

[1]Durability CAE Body & Trim, Volvo Car Corporation, Gothenburg, Sweden
Email: henrik.molker@volvocars.com, Web Page: http://www.volvocars.com
[2]Swerea SICOMP AB, Mölndal, Sweden
Email: Renaud.gutkin@swerea.se, Web Page: http:// http://www.swerea.se/sicomp
[3]Department of Aeronautics, Imperial College, London, United Kingdom
Email: silvestre.pinho@imperial.ac.uk, Web Page: http://www. imperial.ac.uk
[4]Department of Applied Mechanics, Chalmers University of Technology, Gothenburg, Sweden
Email: leif.asp@chalmers.se, Web Page: http://www.chalmers.com

Keywords: Carbon fibre composites, Textile, Local-Global, Failure, Finite Element

Abstract
In this paper, intrabundle failure initiation in NCF reinforced composite materials is predicted based on a finite element model built with shell elements. The full 3D stress state is estimated based on the shell results and used in a state of the art 3D failure criterion. The procedure considers predictions of the transverse shear and normal stresses from stress equilibrium. By using this approach on shell elements, more efficient modelling strategies suited to identify hot spots in larger structures can be pursued.

1. Introduction

To meet energy consumption targets beyond the year 2020, the weight of road vehicles must be reduced. A technology step by introducing Carbon Fibre Reinforced Plastics (CFRP) in vehicle structural parts, mainly body parts, has started in the automotive industry. This relates to the outstanding weight saving potential of these materials compared to metal alternatives. Automotive bodies made from CFRP are considered 50% lighter compared to corresponding steel alternatives and 30% lighter than aluminium alternatives, with similar or better stiffness, durability and crash worthiness properties [1]. More recent studies anticipate a potential weight saving up to 60% [2] or even as much as 70% [3] with CFRP compared to steel. A weight saving of 100 kg corresponds to a decrease of the CO_2-emissions of about 6 gCO_2/km [4].

Traditional modelling within automotive industry for durability aspects uses shell elements for the structural parts, e.g. sheet metal structures. This is because they give a good balance between accuracy and computational effort. For composite materials the strength is either transversely isotropic, e.g. Uni-Directional (UD) reinforced composite materials [5], or orthotropic, e.g. Non-Crimp Fabric (NCF) reinforced composite materials [6], [7]. For such composite reinforcements the assumption of plane stress (neglecting the out of plane stress) is not valid and can cause failure due to unforeseen stresses in integral components, e.g. L-shaped designs, [8].

For structures where large out of plane stresses occur, modelling potentially critical areas with high fidelity models is needed to validate the structure. These models are often made with one solid brick

Excerpt from ISBN 978-3-00-053387-7

(HEX) element for each ply within the laminate. This quickly results in computationally heavy models. Therefore, in large structures with complex geometries, finding these potentially critical areas becomes fundamental.

The focus of the current research is to develop a method for identifying potential hot spots in large composite structures. This is done by extending the output from traditional shell elements with estimations of all stress components based on stress equilibrium. The estimated 3D stress state is then used in State of The Art (SoTA) failure initiation criteria for NCF materials [9]. This set of criteria address the orthotropic strength of NCF materials. In this paper the out-of-plane failure mode for NCF reinforced composite materials will be studied.

Once such a hot-spot criterion is developed, it can then be used for identification of critical areas within an analysis framework for structural components using a global – local approach.

2. 3D failure prediction at ply level in a shell based model

Modelling of composites structures where the full stress tensor is needed results in the need for high fidelity models. This can be either by solid models or user-developed enriched shell elements that are not available in commercial software. Such elements include zig-zag based or higher order deformation theories [10]. Such models have one thing in common, the number of degrees of freedom rapidly increases for layered composite materials.

2.1. Estimation of full 3D stress state at ply level

From 2D shell elements where the in-plane stresses are known, it is possible to estimate the out of plane stresses from a stress equilibrium in all directions. The basic idea is that the stress derivate in all directions need to be in balance according to Eq. (1), without any external forces acting on the studied volume. If this is satisfied, then the out of plane components can be estimated by integration.

$$\begin{cases} \dfrac{\partial \sigma_x}{\partial x} + \dfrac{\partial \tau_{yx}}{\partial y} + \dfrac{\partial \tau_{zx}}{\partial z} = 0 \\ \dfrac{\partial \tau_{xy}}{\partial x} + \dfrac{\partial \sigma_y}{\partial y} + \dfrac{\partial \tau_{zy}}{\partial z} = 0 \\ \dfrac{\partial \tau_{xz}}{\partial x} + \dfrac{\partial \tau_{yz}}{\partial y} + \dfrac{\partial \sigma_z}{\partial z} = 0 \end{cases} \tag{1}$$

From the first two equations, the out of plane shear stresses, τ_{zx} and τ_{zy}, can be calculated from in-plane components. With these known, the out of plane normal stress, σ_z, can be calculated.

A procedure for estimation of the transverse shear stresses in a composite based on first order shear deformation elements has been proposed by Rolfes and Rohwer [11], Eq. (2),

$$\boldsymbol{\tau}_z = \begin{bmatrix} \tau_{zx} \\ \tau_{zy} \end{bmatrix} = -\int_{\xi=0}^{\xi=z} \begin{pmatrix} \sigma_{x,x}^{(k)} + \tau_{yx,y}^{(k)} \\ \sigma_{y,y}^{(k)} + \tau_{xy,x}^{(k)} \end{pmatrix} d\xi \,, \tag{2}$$

where $\sigma_{i,l}^{(k)} = \dfrac{\partial \sigma_i}{\partial l}$ for layer k and $\tau_{ij,l}^{(k)} = \dfrac{\partial \tau_{ij}}{\partial l}$ for layer k.

When the transverse shear stresses are estimated the out of plane stress component, σ_z, can be calculated in a similar approach [12] in Eq. (3),

Excerpt from ISBN 978-3-00-053387-7

$$\sigma_z(z) = -\int_{\xi=0}^{\xi=z} \left(\tau_{xz,x} + \tau_{yz,y}\right) d\xi + p_0 \tag{3}$$

Eq. (3) and Eq. (4) rely on the following assumptions: there are no shear acting on the boundaries, the membrane forces contribution on the transverse shear strains can be neglected and the displacement modes of the element is cylindrical around the *x* and *y* axes of the element.

Using the assumptions of the displacement modes and the neglected membrane forces together with Classical Laminate Theory (CLT) makes it possible to estimate the transverse shear, Eq. (4),

$$\boldsymbol{\tau}_z = \mathbf{f}(z)\mathbf{R} \tag{4}$$

and normal stress, Eq. (5),

$$\sigma_z(z) = -\left[\mathbf{f}_\mathbf{x}^{*\mathbf{T}}(z)\mathbf{R}_{,x} + \mathbf{f}_\mathbf{y}^{*\mathbf{T}}(z)\mathbf{R}_{,y}\right] + p_0 \tag{5}$$

from the transverse shear forces **R** and the derivate of **R´**. The functions **f**(*z*) and **f***(*z*) are based on the stiffness properties of the laminate.

The calculation also uses an updated shear stiffness, **H**. The updated stiffness is based on integration over the thickness taking the different orientations of each individual ply into account. Using the updated stiffness together with the transverse shear strains, **γ**, according to Eq. (6) gives the transverse shear forces,

$$\mathbf{R} = \mathbf{H}\boldsymbol{\gamma} \tag{6}$$

The added cost for this methodology is that second order base functions and results from second order elements are required to determine the derivative of the transverse shear forces according to Eq. (7),

$$\mathbf{R}' = \mathbf{H}\boldsymbol{\gamma}' \tag{7}$$

as the derivate of the shear strains, **γ´**, are required, see further in Rolfes and Rohwer [11].

From this procedure, all the stress components through the thickness of the element are known.

2.2. Failure criteria

SoTA failure criteria for continuous fibre composites, e.g. LaRC05 [13] and Puck [14] for UD composites and a set of the criteria proposed by Molker et al. [9] for NCF reinforced materials, use the full stress tensor to account for stress combinations in all directions.

The presented set of criteria by Molker et al. [9] addresses the orthotropic transverse strength of NCF-reinforced composite materials. Two different failure modes are active for transverse loading. Either failure occurs inside the fibre bundle, interbundle failure, or at the edge of the bundle towards the matrix material, intrabundle failure. The intrabundle failure is predicted with the LaRC05 [13] criterion for matrix failure, while the interbundle failure is predicted with a modified criterion [9] according to Eq. (8),

$$FI_{\mathrm{M,MI}} = \left(\frac{\tau_{\mathrm{T,MI}}}{S_{\mathrm{T,MI}}}\right)^2 + \left(\frac{\tau_{\mathrm{L,MI}}}{S_{\mathrm{L,MI}}}\right)^2 + \left(\frac{\sigma_{\mathrm{N,MI}}}{Z_{\mathrm{T}}}\right)^2 = 1, \; if \; \sigma_{\mathrm{N,MI}} > 0, \tag{8}$$

where the tractions, transverse, $\tau_{\mathrm{T,MI}}$, longitudinal, $\tau_{\mathrm{L,MI}}$, and normal, $\sigma_{\mathrm{N,MI}}$, on the fracture plane are compared against the corresponding allowables, $S_{\mathrm{T,MI}}$, $S_{\mathrm{L,MI}}$ and Z_{T}, see Table 2.

The failure criterion is used on the ply level and requires the full 3D stress state from which the tractions, $\tau_{\mathrm{T,MI}}$, $\tau_{\mathrm{L,MI}}$ and $\sigma_{\mathrm{N,MI}}$, on the fracture plane are calculated.

Excerpt from ISBN 978-3-00-053387-7

3. Test case

A rectangular plate, that is supported along the boundaries according to Eq. (9), is subjected to a double cosine pressure load with the magnitude, p_0, of +20 MPa at the centre of the plate, as shown in Figure 1. A similar load case is studied by Rolfes et al. in [12]. The dimensions of the plate is such that the height is set to unity and the ratios between a/h = 20, and a/b = 1. The model has a $[90_2 / 0_2]_S$ layup with a ply thickness of 0.1875 mm.

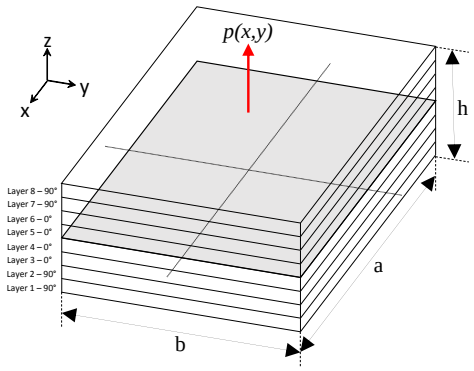

Figure 1. Illustration of load case and composite model.

$$
\begin{aligned}
u_x\left(y=\pm\frac{b}{2}\right)&=0\\
u_y\left(x=\pm\frac{a}{2}\right)&=0\\
u_z\left(x=\pm\frac{a}{2},y=\pm\frac{b}{2}\right)&=0\\
p(x,y)&=p_0\cos\left(\frac{\pi x}{a}\right)\cos\left(\frac{\pi y}{b}\right)
\end{aligned}
\qquad (9)
$$

This load case has been chosen as it is similar to what has been presented before and as it creates an out-of-plane stress component even for a flat specimen. The magnitude of the pressure, p_0, is chosen to achieve a stress state with high out-of-plane normal stresses that potentially can create out of plane failure for NCF reinforced composites.

The material used in the model is a NCF reinforced composite made from HTS45 fibres and LY556 resin from Bru et al. [6]. Elastic and strength properties are given in Table 1 and Table 2, respectively.

Table 1. Elastic properties of the NCF reinforced composite on homogenised ply level [6].

E_{11} (GPa)	E_{22} (GPa)	E_{33} (GPa)	ν_{12}	ν_{13}	ν_{23}	G_{12} (GPa)	G_{13} (GPa)	G_{23} (GPa)
136.0 [a)]	9.2 [a)]	8.0 [a)]	0.29	0.29	0.43	4.3	3.7	2.8

[a)] Average of tension and compression.

Table 2. Strength properties of the NCF reinforced composite on homogenised ply level [6].

Y_T (MPa)	Y_T^{is} (MPa)	Y_C (MPa)	Z_T (MPa)	Z_C (MPa)	S_L (MPa)	S_L^{is} (MPa)	S_T^{is} (MPa)	α_0 (deg)	G_{IC} (J/m^2)	G_{IIC} (J/m^2)
29	46	130	15	202	78	94	49	62	149	690

3.1. Shell model

The shell model is analysed using second order FSDT elements based on Mindlin-Reissner plate theory [15]. The difference to a standard element is that the shear stiffness is taking the orientation of each individual layer into account, instead of using a constant shear correction factor, see further in Rolfes and Rohwer [11]. The transverse shear stresses will be very much dependent on the transverse

Excerpt from ISBN 978-3-00-053387-7

shear stiffness, as can be seen from Eq. (5) and Eq. (6). The shell model has an element size approximately equal to (1.43 x 1.43 mm) which gives 21 x 21 elements.

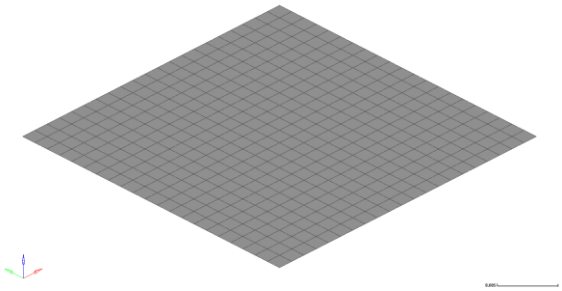

Figure 2. Illustration of shell model and mesh size.

3.2. 3D solid models

To validate the results from the shell model, different solid models have been analysed. One model to verify the estimated stress distribution, called reference 3D model, and one model to verify the predicted failure index, called standard 3D model. The solid models are built using first order solid HEX-elements with an aspect ratio of three. The reference 3D model for the stress distributions are built using four elements over the thickness of each ply. This gives an element size approximately equal to (0.139 x 0.139 x 0.046 mm) resulting in 212 x 212 x 32 elements.

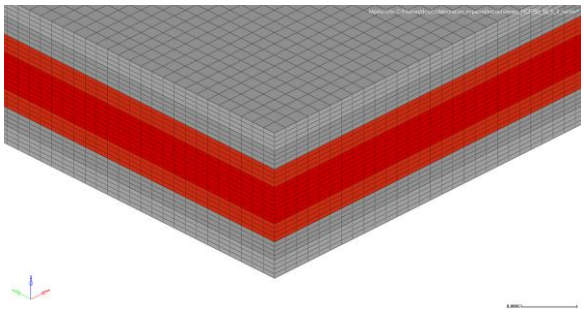

Figure 3. Illustration of the reference 3D model and mesh size, magnified by a factor of 10.

The standard 3D model for the failure prediction uses only one element over the ply thickness, as in Molker et al. [16] for the implementation of the failure criteria. This gives an element size approximately equal to (0.555 x 0.555 x 0.185 mm) resulting in 53 x 53 x 8 elements.

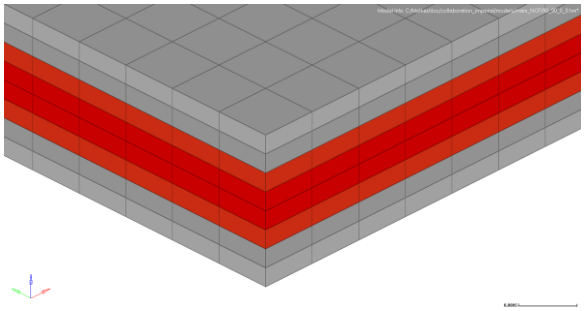

Figure 4. Illustration of the standard 3D model and mesh size, magnified by a factor of 10.

Excerpt from ISBN 978-3-00-053387-7

4. Results

4.1. Correlation of stresses between the different models

The resulting transverse normal stress distributions from the different models can be found in Figure 5. The stresses are shown for the midpoint of the plate through the thickness.

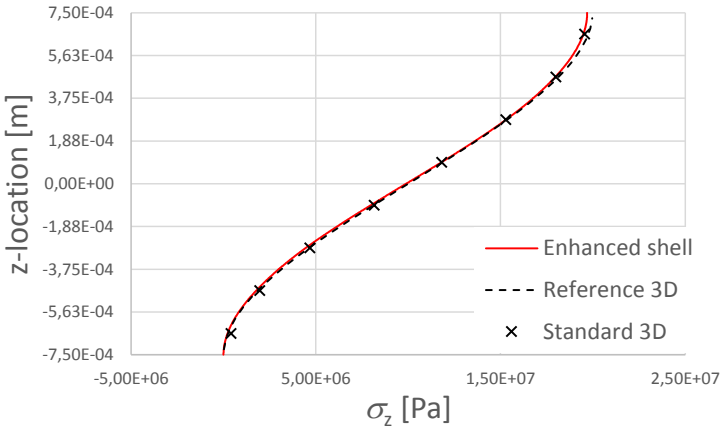

Figure 5. Normal stress distributions, σ_z, through the thickness of the laminate at the centre. The red solid line is the estimated stress distribution from the enhanced shell elements. The dashed black line is the distribution from the reference 3D model. The cross-marks are the stresses at the element centroids for the standard 3D model.

4.2. Failure initiation in shell model and standard 3D model

Failure initiation predictions are made for intrabundle failure for both stress states obtained from the shell model and from the standard 3D model. As the failure initiation prediction is made at discrete points, a representative value needs to be defined from the shell model. The results used for the stress state from the shell model within each ply is the maximum absolute value of each stress component. The standard 3D model uses an implemented subroutine from [16] for prediction of failure initiation in NCF reinforced materials that predicts the failure at each material point in the model. The difference between which stresses that are used for the failure prediction can be seen in Figure 6.

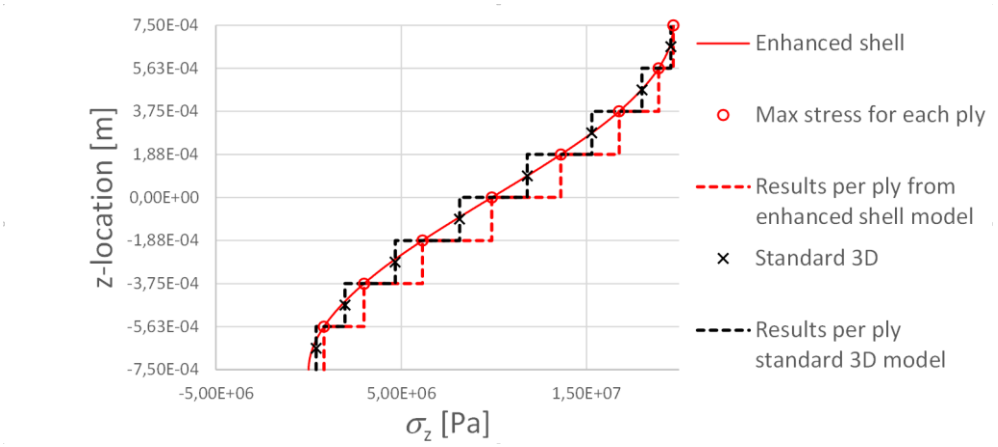

Figure 6. For the enhanced shell model, the normal stress distribution is marked with a solid red line, the maximum within each ply with a red circle and the extracted distribution for failure initiation with a dashed red line. For the standard 3D model, the maximum within each ply is marked with a black cross and the distribution for failure initiation with a dashed black line.

Excerpt from ISBN 978-3-00-053387-7

The predicted failure indexes, for each for ply in both the shell model, using Eq. (8), and the standard 3D model, using the subroutine, are presented in Table 3.

Table 3. Failure indexes for intrabundle failure, $(FI_{M,MI})$, for the centre element and for each ply based on the enhanced shell results and the standard 3D model.

Ply nr.	Shell model	Standard model
8	1.72	1.74
7	1.59	1.48
6	1.25	1.06
5	0.82	0.64
4	0.43	0.31
3	0.17	0.11
2	0.04	0.05
1	0.00	0.05

5. Discussion and conclusion

The presented procedure of estimating all of the stresses from a shell element makes it possible to use SoTA 3D based failure analysis with large models for composite materials. This can be crucial for composite materials that shows an orthotropic strength behaviour, e.g. NCF reinforced composites.

The predicted failure indexes from the shell model are conservative for most plies in relation to the results from the standard 3D model. The main reason for this is that the maximum stress within the ply is used, indicated by red circles in Figure 6. This is greater than the stress used within the standard 3D model, which uses the stress at the material points, in this case the centre of the element, marked by black crosses in Figure 6.

For the current set up the result from the enhanced shell model will be more accurate as better resolution through the thickness is available. However, this is only true if the quality of calculated 3D stresses in the shell model are accurate enough. A study of factors that could influence the accuracy of the enhanced shell model is therefore desired

Using the approach by Rolfes et al. [12] for estimating the transverse shear and normal components in the stress tensor makes it possible to retrieve the full stress tensor from a layered shell element. This can be done by updating the transverse shear stiffness of existing second order shell elements based on FSDT theory. Such elements are available in most commercial finite element software.

By doing this, accurate estimations of the transverse shear and normal stress components can be achieved, as shown in Figure 5, by post processing the nodal results using second order base functions.

Applying the failure criterion for intrabundle failure [9] to the estimated stresses from the shell model yields accurate predictions as shown in Table 3.

These predictions can be used for identification of hot spot areas on large structures to a moderate increase in computational cost due to the need of second order shell elements.

6. Acknowledgments

The work is funded through Volvo Car Industrial PhD program (VIPP) and the Swedish Research Council (VR) 2012-4320. Financial support from Vinnova, via LIGHTer SRA1 Modelling, is gratefully acknowledged.

Excerpt from ISBN 978-3-00-053387-7

7. References

[1] BMW Media Material, "Mobility of the future.," in *BMW Group Innovation Days 2010*, 2010.
[2] "Carbon-Fiber Composites for Cars." [Online]. Available: http://www.web.ornl.gov/info/ornlreview/v33_3_00/carbon.htm. [Accessed: 20-Mar-2014].
[3] "Renewable, Low-Cost Carbon Fiber for Lightweight Vehicles: Summary Report. Detroit, MI: U.S. Department of Energy (US); 2013 October."
[4] "Briefing Reducing CO 2 and fuel consumption from new cars: Assessing the near-term technology potential in the EU," 2013.
[5] D. Zenkert and M. Battley, *Foundations of Fibre Composites*, 2nd ed. Stockholm: KTH FLYG, 2012.
[6] T. Bru, P. Hellström, R. Gutkin, D. Ramantani, and G. Peterson, "Characterisation of the mechanical and fracture properties of a uni-weave carbon fibre/epoxy non-crimp fabric composite," *Data in Brief*, vol. 6. pp. 680–695, 2016.
[7] R. Olsson, "Experimental observations on the orthotropic transverse strength of non-crimp fabrics composites [TN15006].," Piteå, 2015.
[8] P. C. Paul, C. R. Saff, K. B. Sanger, M. A. Mahler, H. P. Kan, and E. F. Kautz, "Out of plane analysis for composite structures," *Nasa Tech. Rep. 19920023283*, pp. 263–279, 1990.
[9] H. Molker, D. Wilhelmsson, R. Gutkin, and L. E. Asp, "Orthotropic criteria for transverse failure of non-crimp fabric-reinforced composites," *J. Compos. Mater.*, 2015.
[10] T. Kant and K. Swaminathan, "Estimation of transverse/interlaminar stresses in laminated composites – a selective review and survey of current developments," *Compos. Struct.*, vol. 49, no. 1, pp. 65–75, 2000.
[11] R. Rolfes and K. Rohwer, "Improved transverse shear stresses in composite finite elements based on first order shear deformation theory," *Int. J. Numer. Methods Eng.*, vol. 40, no. 1, pp. 51–60, Jan. 1997.
[12] R. Rolfes, K. Rohwer, and M. Ballerstaedt, "Efficient linear transverse normal stress analysis of layered composite plates," *Comput. Struct.*, vol. 68, no. 6, pp. 643–652, 1998.
[13] S. Pinho, R. Darvizeh, P. Robinson, C. Schuecker, and P. Camanho, "Material and structural response of polymer-matrix fibre-reinforced composites," *J. Compos. Mater.*, vol. 46, no. February, pp. 2313–2341, 2012.
[14] A. Puck and H. Schumann, "Failure analysis of FRP laminates by means of physically based phenomenological models," *Compos. Sci. Technol.*, vol. 62, pp. 1633–1662, 2002.
[15] J. N. Reddy, *Theory and Analysis of Elastic Plates and Shells, Second Edition*. Boca Raton: CRC Press, 2006.
[16] H. Molker, R. Gutkin, and L. E. Asp, "Implementation of failure criteria for orthotropic non crimp fabric composite structures," in *V ECCOMAS Thematic Conference on the Mechanical Response of Composites - COMPOSITES 2015*, 2015.

Excerpt from ISBN 978-3-00-053387-7